NANO LETTERS

2008
Vol. 8, No. 1
241−245

Graphene NanoFlakes with Large Spin

Wei L. Wang, Sheng Meng, and Efthimios Kaxiras*

Department of Physics and School of Engineering & Applied Sciences, Harvard University, Cambridge, Massachusetts 02138

Received October 4, 2007; Revised Manuscript Received November 8, 2007

ABSTRACT

We investigate, using benzenoid graph theory and first-principles calculations, the magnetic properties of arbitrarily shaped finite graphene fragments to which we refer as graphene nanoflakes (GNFs). We demonstrate that the spin of a GNF depends on its shape due to topological frustration of the π-bonds. For example, a zigzag-edged triangular GNF has a nonzero net spin, resembling an artificial ferrimagnetic atom, with the spin value scaling with its linear size. In general, the principle of topological frustration can be used to introduce large net spin and interesting spin distributions in graphene. These results suggest an avenue to nanoscale spintronics through the sculpting of graphene fragments.

Carbon-based magnetism[1] is intriguing, especially when derived from graphene, a material touted as the basis for next generation electronic and spintronics devices.[2] The recent discovery of true two-dimensional (2D) graphene crystals[3,4] has stimulated intensive study of this system revealing many of its exciting properties such as massless quasi-particles,[5] high mobility and coherence,[3] room-temperature quantum hall effect,[6] and half-metallicity[7] to name but a few. These properties are significant not only from a fundamental perspective, but also for technological applications. To date, most studies on graphene have been focused on its mesoscopic properties related to electronic conductivity with only a few exceptions explicitly addressing the intrinsic magnetic properties of certain graphene-derived structures, namely the graphene nanoribbons (GNRs).[7−12] The zigzag edges of GNRs introduce a localized edge state contributing to a flat band at the Fermi level. These edge states are spin polarized and localized on either side of the GNR, with antiparallel spins for a total spin of zero.[11]

A GNR has one-dimensional (1D) straight edges, which can be considered as a special case of the more general, arbitrarily shaped graphene fragments that are finite in both dimensions to which we refer as graphene nanoflakes (GNFs). Understanding the properties of GNFs is important because the basic functional components of future electronics or spintronics devices will need to be at the nanometer scale to uphold the trend of increased performance with miniaturization (Moore's law). In fact, very recent experiments have achieved graphene features at the scale of tens of nanometers.[2] Meanwhile, quantum confinement and variations of the edges in GNFs give rise to rich electronic and magnetic properties, as we show below. The previously reported magnetic properties of GNRs[7−12] are merely the tip of the iceberg for magnetic applications involving graphene fragments.

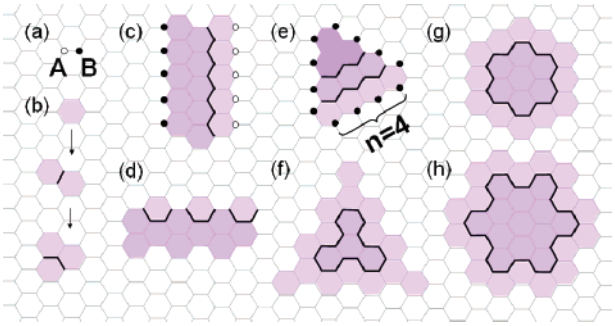

Figure 1. Various types of graphene nanoflakes stitched up from smaller subflakes (darker shade). Black lines are stitches, and the hydrogen termination along the edges is not shown. (a) The two sublattice sites *A* (white) and *B* (black) of graphene. (b) GNFs constructed by stitching up *A*-*B* balanced hexagons; the resultant triangular GNF has $N_A = 7$, $N_B = 6$, and total spin 0.5. (c) GNF that corresponds to zigzag-edged GNRs. (d) GNF that corresponds to armchair-edged GNRs. (e) Zigzag-edged triangular GNF with four edge carbon atoms. (f) Armchair-edged triangular GNF. (g) Zigzag-edged hexagonal GNF. (h) Armchair-edged hexagonal GNF.

In this paper, we characterize, using benzenoid graph theory and first-principles electronic structure calculations, arbitrarily shaped hydrogen-terminated GNFs, starting with the 3-fold and 6-fold highly symmetric types, as well as those related to finite GNRs; these shapes are shown in Figure 1 panel c to panel h. All these structures have zero intrinsic spin except the one in Figure 1e, the zigzag-edged triangular GNF in which a linear-scaling net spin arises due to topological frustration of the π-bonds. We also discuss the possibilities for applying the principle of topological frustration in the design of structures with large spin and in the context of circuits for spintronics applications.

* To whom correspondence should be addressed.

10.1021/nl072548a CCC: $40.75
Published on Web 12/05/2007

In electronic structure calculations based on the tight-binding approximation (TBA), if only nearest-neighbor hopping is considered and the on-site energy set to zero then the secular equation reads $Dx = Ex$ with D being the hopping matrix and E the eigenvalues. The dimension of D is equal to the number of orbitals, and D has as nonzero elements only those coupling orbitals on adjacent atoms. In special cases, D becomes singular and zero eigenvalues arise, which are called nonbonding states (NBSs); the atomic structure corresponding to this case is referred to as a "singular molecular graph". In a singular graph, topological frustration occurs, that is, all the π-bonds cannot be satisfied simultaneously, implying possible spin-aligned singly occupied molecular orbitals (SOMOs) which can arise from degeneracy at the Fermi level. Characterizing singular graphs has been a long-standing problem in graph theory. In 1985, the first structural identification of singular benzenoid graphs was achieved[13] but it took another 20 years to prove a theorem[14] that establishes rigorously the connection between structural characteristics and the eigenvalue distribution. Applied to a GNF consisting of benzenoid rings and bounded by a single topological circuit, this theorem reveals that the maximum number of pairwise nonadjacent vertices α and edges β of the graph G are given by $\alpha(G) = \beta(G) + \eta(G)$ and $\beta(G) = \theta(G) = \nu(G)$ where θ, ν, and η are the number of positive, negative and zero eigenvalues of D, respectively; η is also called the "nullity" and is equal to the number of NBSs. We may therefore write the total spin as

$$S = \eta/2 = (\alpha - \beta)/2 = \alpha - N/2 \quad (1)$$

where N is the total number of vertices that is equal to the sum of θ, ν, and η.

A GNF consists of a bipartite hexagonal lattice, which has two subsets of sites, A and B, with bonds only between atoms belonging to different subsets. Each sublattice with a population of N_A or N_B, naturally makes a nonadjacent set, but in general, $N_A \leq \alpha$ and $N_B \leq \alpha$. We first focus on a special case where

$$\alpha(G) = \max\{N_A(G), N_B(G)\} \quad (2)$$

We prove that all types of GNFs shown in Figure 1b−g fall into this category. The proof is recursive and takes the zigzag-edged triangular GNF shown in Figure 1e (for which $N_B > N_A$ holds) as an example. For the GNF with $n = 2$, exhaustive search yields that $\alpha = N_B$. We next show that if $\alpha = N_B$ holds for any integer $n \geq 2$ then it holds for $n + 1$. The graph of size $n + 1$ is constructed by starting with the graph G of size n and adding to one side of it a line graph S, for which we must have $\alpha(S) = n + 2 = N_B(S)$. But in general, $\alpha(S + G) \leq \alpha(S) + \alpha(G)$, which can be proved by reductio ad absurdum. Therefore, we have $\alpha(S + G) \leq N_B(S) + N_B(G) = N_B(S + G)$, where the equal sign applies because any set of B vertices are nonadjacent. This completes the proof. The proofs are similar for the other types of GNFs shown in Figure 1.

As long as eq 2 holds for a GNF, its nullity can be easily counted by breaking the GNF apart into subflakes and stitching them up again, as shown in Figure 1. We define a stitch as a single path of bonds that merges two subflakes, which is either even if it contains an even number of atoms or odd otherwise. Clearly, there are equal numbers of A and B sites in an even stitch but one additional A or B site in an odd stitch. Therefore, an odd stitch creates or annihilates exactly one NBS while an even one leaves the total number of NBSs unchanged according to eqs 1 and 2.

With this counting rule, we can construct GNFs with nonzero spin by stitching together hexagonal units that by themselves have zero spin; the simplest example is shown in Figure 1b, where a minimum GNF with spin 0.5 is constructed. An extension of this is shown in Figure 1e where, starting with a zigzag-edged triangular GNF with n-edge carbon atoms and adding to it an additional layer of A-B balanced sites (lighter color hexagons), it produces a zigzag-edged triangular GNF with $n + 1$ edge carbon atoms. This introduces one more B site than A site into to the system therefore the total nullity is $\eta = n - 1$, indicating the net spin scales linearly as the linear size of the GNF. In contrast to zigzag-edged triangular GNFs, a graphene nanoribbon regardless of its size and edge type must have zero nullity because it can always be constructed from A-B balanced subflakes with even stitches, as illustrated in Figure 1c,d. Therefore, the flat band edge states in a GNR are fundamentally different form the NBSs of a GNF. The former asymptotically approach the Fermi level due to size effects, while the latter is associated with singularities of the hopping matrix D. It is this difference that eventually leads to the result that a GNR must have zero net spin, while a GNF can accommodate a large spin. This point is evident when looking at the two parallel edges of a zigzag-edged GNR where the type of sublattice on either side must be different. In contrast, the orientation of edges in a zigzag-edged triangular GNF makes it possible that all atoms on the edges belong to the same sublattice, which breaks the symmetry between sublattices and gives rise to large spin according to eqs 1 and 2. Similar to the finite GNRs, the rest of GNF types from Figure 1 panel f to panel h have $N_A = N_B$ and thus $\eta = 0$. Clearly, the existence of NBSs in zigzag-edged triangular GNFs and its absence from the other types of GNFs stems from the symmetry of the structures with respect to the two sublattices of graphene. In all shapes but the zigzag-edged triangular GNFs, it is possible to transform A sites to B sites by a point group operation.

To justify these arguments beyond the level of graph theory, we use first-principles electronic structure calculations within density functional theory (DFT). We employ the SIESTA[15−17] code with all GNFs relaxed by optimizing the bond lengths until the force on each atom is smaller in magnitude than 0.04 eV/Å. During the optimization, the electronic ground state is solved self-consistently by using norm-conserving pseudopotentials to represent the atomic cores and a double-ζ plus polarization basis of localized orbitals with an energy cutoff of 70 Ry. For the exchange-correlation functional, we use the local density approximation (LDA) and the spin-polarized (LSDA) version where appropriate. Within the nonspin-polarized LDA, the NBSs are

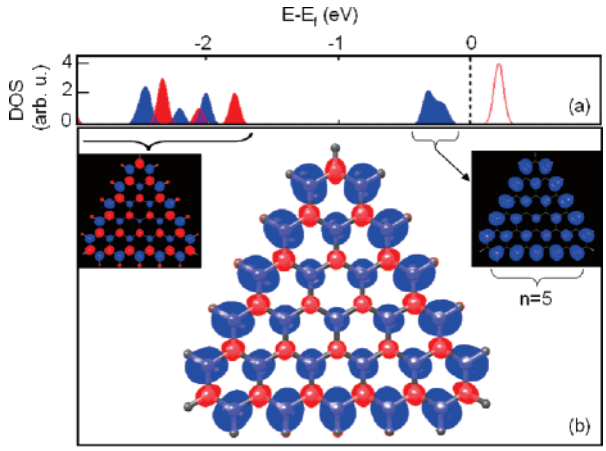

Figure 2. Zigzag-edged triangular graphene flakes with ferrimagnetic order and linearly scaling net spin. (a) Density and filling of the spin-polarized states: blue and red correspond to up (u) and down (d) spin. (b) Spatial distribution of the spin density difference $[\rho_u(r) - \rho_d(r)]/2$ over the artificial atom, which is the sum of the spin density shown in the two smaller insets. Right inset: spin density of the SOMOs. Left inset: spin density of all other occupied orbitals. Spin density contours are shown at the value of 0.0025/Å^3.

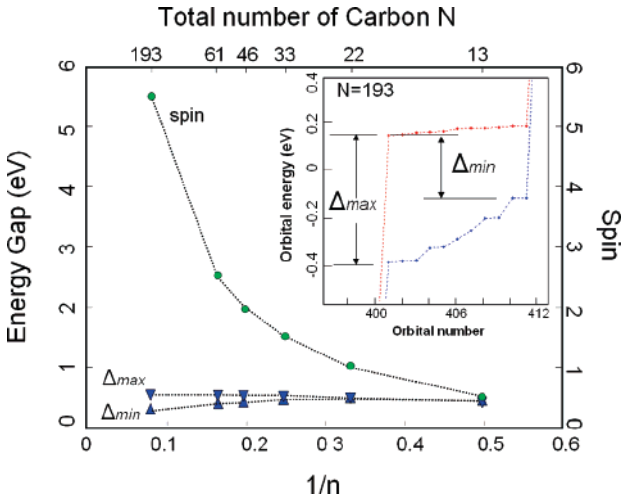

Figure 3. Scaling of spin and energy gap with the inverse linear size ($1/n$) of zigzag-edged triangular graphene flakes. Δ_{max} and Δ_{min} are the maximum and minimum energy gaps from the SOMOs to the lowest unoccupied molecular orbital, as shown in the inset; dotted lines are guides to the eye.

still present after taking into account structural relaxation and all the interactions beyond the nearest neighbors (which are automatically taken into account in the DFT calculations), consistent with previous calculations[18] within the TBA. This is not surprising because the homogeneous hopping matrix is not a necessary condition for the matrix to be singular. Rather, it is the topology constraint that gives rise to the NBSs. These NBSs are half filled and behave like the outer shell of a ferromagnetic atom, which is not stable when spin is taken into account. The exchange interaction requires the spin in these orbitals to be maximized, similar to Hund's rule for atoms. As an example, the LSDA calculation of the structure in Figure 2 shows that the degenerate NBSs split and create an energy gap of 0.40 eV and a total spin of 2. The energy difference between spin-polarized and spin-unpolarized ground states is 0.48 eV and in favor of the polarized state.

With the NBSs split into two spin states, the SOMOs with majority spin (assigned as spin up) are localized exclusively on the majority subset of sites (Figure 2b, right inset). The asymmetry in the spin of these orbitals lifts the degeneracy on the remaining orbitals (Figure 2a). Meanwhile, due to the asymmetry in spatial distribution, the remaining spin-up orbitals are attracted to the majority subset of the sites by the exchange interaction while the spin-down orbitals are repelled from the majority subset and attracted to the minority subset of the sites (Figure 2b, left inset). The whole system thus develops a ferrimagnetic order with opposite spins on the two subsets of the sites and with the total spin-up larger than the total spin-down by a net amount equal to $(n - 1)/2$. This value scales with the linear size of the GNF as predicted by graph theory.

For zigzag-edged triangular GNFs of nanometer size, the split of the NBSs creates an energy gap of 0.3−0.5 eV at the Fermi level, as shown in Figure 3. Therefore the spin alignment should be stable at room temperature, consistent with theoretical results on high-temperature magnetism of sp electrons.[19] When the linear size of the triangular graphene flake increases beyond the nanometer scale, the minimum energy gap between the SOMOs and the lowest unoccupied molecular orbital decreases and approaches zero, which corresponds to the properties at the Dirac point in extended 2D graphene. However, the maximum energy gap, as defined in Figure 3, remains ∼0.5 eV, and therefore it should be possible to measure the magnetic moment at the edge of the triangular graphene flake even beyond the nanoscale at room temperature. It is well known that graphene is subject to weaker spin−orbit coupling and hyperfine interactions than semiconductors, which lead to increased coherence time of the spin states.[20] This property, together with the scalability of total spin and its stability up to room temperature, renders the artificial ferrimagnetic atom made from graphene an excellent candidate for spintronic devices such as spin memory, transistors, and perhaps solid-state qubits.

From a chemical point of view, these hydrogen-terminated graphene triangles can be called colossal hydrocarbon radicals except that the former are not as reactive because in a conjugated π-system the delocalization of the unpaired spin orbital substantially lowers its energy. The enhanced stability of such systems has been noted in previous theoretical studies on small model graphene systems[21] and the zigzag edges of GNRs.[22] Synthesis of stable polymer radicals with large spin has been a long standing goal in chemistry and some successful experiments have produced π-conjugated polymers with molecular spin as high as $S = 5000$.[23]

However, with chemical synthesis being a traditional bottom-up approach this way of obtaining large-spin molecules is limited by the complex reaction pathways available. Meanwhile, the harsh reaction conditions and the interactions between the radicals may easily destroy the spin properties, for instance, through oligomerization. In contrast, a GNF with

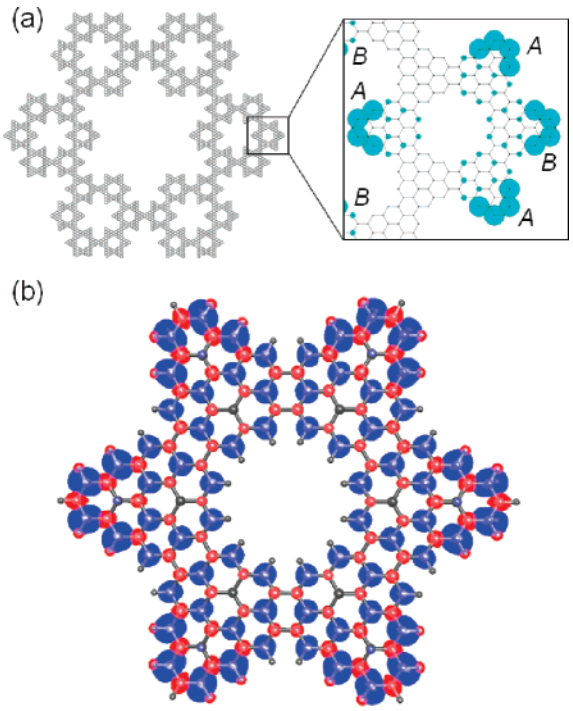

Figure 4. Fractal structure of a "Star of David" graphene nanoflake in which the spin increases with the fractal level. (a) The fractal GNF and the distribution of the spin density in one of the subunits from TBA calculations. Each region is marked with *A* or *B*, indicating the switch of sublattice where the majority spin resides. (b) Spin density difference $[\rho_u(r) - \rho_d(r)]/2$ (blue = positive, red = negative) over a single subunit of the structure in (a) from first-principles calculations of the relaxed structure. The calculated total spin is 2.35 instead of the value 3.0 expected from TBA calculations. Spin density contours are shown at the value of 0.0025 /Å^3.

large spin can in principle be carved from graphene through lithography, which provides an alternative top-down approach that avoids these complications. Our preceding analysis indicates that the highest reported spin in conjugated polymers may be easily exceeded in a graphene flake of submicron size. Although defects may reduce the net spin, it is clear from eq 1 that the nullity of the system is not reduced by defects in any dramatic way, that is, the total spin is not sensitive to defects as long as they are not so abundant that the entire edges of the flake become irregular.

It is important to note that the large spin demonstrated in zigzag-edged triangular GNFs is only a special case of eq 2, which in turn is a special case of eq 1 where the number of maximum nonadjacent sites is not necessarily equal to N_A or N_B. In the latter case, large spin states may be generated much more efficiently. One such example shown in Figure 4 is based on the "Star of David" shape. The structure is fractal and generated by repeatedly overlapping two triangles in opposite direction and removing the overlap portion. The structure has a fractal dimension $\log(1/6)/\log(1/3) = 1.62$, the logarithm ratio of the number-of-atoms fraction and linear-size fraction between successive self-similar levels. The total spin increases exponentially with the fractal level q as $S_q = S_0 2^q$, where S_0 is the spin of the initial graphene triangle. The increase of total spin is due to the increase of boundary length, a hallmark of fractal structures, which here

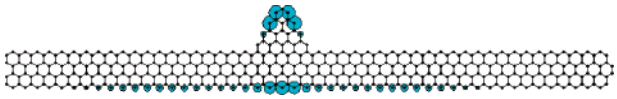

Figure 5. An example of a GNF attached to a GNR, forming a possible spintronic component. The net spin density distribution shown in color is projected from the nonbonding states obtained from TBA calculations on the finite GNR model system shown (see text for details).

increases the possibility of topological frustration of the π-bonds. The set of maximum nonadjacent atoms consists of both *A* and *B* sublattices, switching sublattice index from one region to the next, as shown in the inset of Figure 4a. Therefore, although there is an equal number of *A* and *B* atoms, α is much greater than the half population of the total atoms, resulting in a nullity and spin that is proportional to the total number of the star branches.

Another example of topological frustration that may be of practical interest is shown in Figure 5. It consists of a combination of zigzag-edged triangular GNF with a conducting zigzag-edged GNR that might serve as an electronic or spintronic circuit component. TBA calculations show that the net spin density due to the introduction of the GNF protrusion, not including the antiparallel coupled spin of the finite-GNR edge states, is localized on the GNF protrusion with a small spread on the other side of the ribbon, making it an interesting candidate of a spin memory or spin filter device. Circuits made of such components in principle can be carved out of a single graphene layer through a unified planner process using electron-beam or scan probe microscopy lithography.

In conclusion, we have characterized the spin properties of arbitrarily shaped graphene nanoflakes. We showed that linear-scaling spin arises in zigzag-edged triangular graphene nanoflakes through topological frustration. This principle further suggests a multitude of ways of carving patterns out of a graphene plane (such as dots, stripes, and circuits) with desired spin distribution. These results open the door to spintronic nanoscale devices by sculpting graphene fragments and exploiting the shape dependence of magnetic properties.

Note added in proof. After completion of the present work, we became aware of recent related works by J. Fernndez-Rossier et al.,[24] O. Hod et al.,[25] and M. Ezawa[26] on the spin properties of triangular, hexagonal, and ribbonlike finite graphene fragments. The results reported in these works are consistent with our eq 2, which is a special case of the general principle expressed by our eq 1.

References

(1) Makarova, T. L. *Semiconductors* **2004**, *38* (6), 615−638.
(2) Geim, A. K.; Novoselov, K. S. *Nat. Mater.* **2007**, *6* (3), 183−191.
(3) Novoselov, K. S.; Geim, A. K.; Morozov, S. V.; Jiang, D.; Zhang, Y.; Dubonos, S. V.; Grigorieva, I. V.; Firsov, A. A. *Science* **2004**, *306* (5696), 666−669.
(4) Meyer, J. C.; Geim, A. K.; Katsnelson, M. I.; Novoselov, K. S.; Booth, T. J.; Roth, S. *Nature* **2007**, *446* (7131), 60−63.
(5) Novoselov, K. S.; Geim, A. K.; Morozov, S. V.; Jiang, D.; Katsnelson, M. I.; Grigorieva, I. V.; Dubonos, S. V.; Firsov, A. A. *Nature* **2005**, *438* (7065), 197−200.
(6) Novoselov, K. S.; Jiang, Z.; Zhang, Y.; Morozov, S. V.; Stormer, H. L.; Zeitler, U.; Maan, J. C.; Boebinger, G. S.; Kim, P.; Geim, A. K. *Science* **2007**, *315* (5817), 1379−1379.

(7) Son, Y. W.; Cohen, M. L.; Louie, S. G. *Nature* **2006**, *444* (7117), 347−349.
(8) Fujita, M.; Wakabayashi, K.; Nakada, K.; Kusakabe, K. *J. Phys. Soc. Jpn.* **1996**, *65* (7), 1920−1923.
(9) Nakada, K.; Fujita, M.; Dresselhaus, G.; Dresselhaus, M. S. *Phys. Rev. B* **1996**, 54, 17954.
(10) Owens, F. J. *Mol. Phys.* **2006**, *104* (19), 3107−3109.
(11) Son, Y. W.; Cohen, M. L.; Louie, S. G. *Phys. Rev. Lett.* **2006**, *97* (21), 216803.
(12) Hod, O.; Barone, V.; Peralta, J. E.; Scuseria, G. E. *Nano Lett.* **2007**, *7* (8), 2295−2299.
(13) Gutman, I.; Brunvoll, J. *Advances in the theory of benzenoid hydrocarbons II*; Springer-Verlag: Berlin, 1992; p 226.
(14) Fajtlowicz, S.; John, P. E.; Sachs, H. *Croat. Chem. Acta* **2005**, *78* (2), 195−201.
(15) Ordejon, P. *Phys. Status Solidi B* **2000**, *217* (1), 335−356.
(16) Artacho, E.; Sanchez-Portal, D.; Ordejon, P.; Garcia, A.; Soler, J. M. *Phys. Status Solidi B* **1999**, *215* (1), 809−817.
(17) SanchezPortal, D.; Artacho, E.; Soler, J. M. *J. Phys.: Condens. Matter* **1996**, *8* (21), 3859−3880.
(18) Yamamoto, T.; Noguchi, T.; Watanabe, K. *Phys. Rev. B* **2006**, *74* (12), 121409.
(19) Edwards, D. M.; Katsnelson, M. I. *J. Phys.: Condens. Matter* **2006**, *18* (31), 7209−7225.
(20) Trauzettel, B.; Bulaev, D. V.; Loss, D.; Burkard, G. *Nat. Phys.* **2007**, *3* (3), 192−196.
(21) Peralta-Inga, Z.; Murray, J. S.; Grice, M. E.; Boyd, S.; O'Connor, C. J.; Politzer, P. *J. Mol. Struct.* **2001**, *549*, 147−158.
(22) Jiang, D. E.; Sumpter, B. G.; Dai, S. *J. Chem. Phys.* **2007**, *126* (13), 124701.
(23) Rajca, A.; Wongsriratanakul, J.; Rajca, S. *Science* **2001**, *294* (5546), 1503−1505.
(24) Fernndez-Rossier, J.; Palacios, J. J. *Phys. Rev. Lett.* **2007**, *99*, 177204.
(25) Hod, O.; Barone, V.; Scuseria, G. E. arXiv.org, 0709.0938v2 2007; http://arxiv.org/ (accessed November 1, 2007).
(26) Ezawa, M. arXiv.org, 0709.2066v1 2007 and 0707. 0349v1 2007; http://arxiv.org/ (accessed November 1, 2007).

NL072548A